

# Global evidence for a consistent spatial footprint of intra-urban centers

Shuai Pang,<sup>1</sup> Junlong Zhang,<sup>1</sup> Yu Liu,<sup>1,2</sup> and Lei Dong<sup>1,2</sup>

<sup>1</sup>*Institute of Remote Sensing and Geographical Information Systems,  
School of Earth and Space Sciences, Peking University, Beijing 100871, China*  
<sup>2</sup>*Ordos Research Institute of Energy, Peking University, Ordos 017000, China*

Urban space is highly heterogeneous, with population and human activities concentrating in localized centers. However, the global organization of such intra-urban centers remains poorly understood due to the lack of consistent, comparable data. Here we develop a scalable geospatial framework to identify intra-urban activity centers worldwide using nighttime light observations. Applying this approach to more than 9,500 cities, we construct a high-resolution global dataset of over 15,000 centers. We uncover a striking regularity: despite vast differences in city size, regional development, and population density, the built-up area associated with individual centers remains remarkably consistent. Across cities, total urban area scales proportionally with the number of centers, yielding a stable mean spatial footprint. This regularity holds at the micro-scale, where Voronoi-based service areas exhibit a characteristic size that is persistent across countries and independent of local population concentration. As a geometric consequence, this polycentric multiplication maintains stable average distances to the nearest center as cities expand, preventing the accessibility decay inherent in monocentric growth. These findings reveal a universal organizing principle whereby urban expansion is accommodated through the replication of activity centers with a consistent spatial extent, providing a new empirical foundation for understanding the nature of urban growth.

## INTRODUCTION

Cities, despite occupying a minuscule fraction of the Earth’s terrestrial surface [1], function as the primary engines of global population concentration, economic output, and innovation [2–6]. Within these urban agglomerations, human activities are far from uniformly distributed; instead, they exhibit a highly heterogeneous spatial structure, gravitating toward localized activity centers [7]. Identifying these internal centers is fundamental to understanding the spatial logic of cities, as they govern population distribution [8, 9], rent gradients [10], housing prices [11], traffic flows [12], and service accessibility [13–15]. Classically, Christaller’s Central Place Theory envisioned urban systems organize into a hierarchical spatial grid, where centers serve discrete hinterlands to minimize travel costs and maximize service efficiency. Yet, while such theoretical frameworks suggest an orderly partitioning of space, global empirical evidence for a universal spatial unit of intra-urban organization has remained elusive.

This knowledge gap stems largely from the lack of a consistent and scalable methodology to delineate intra-urban centers globally. Existing studies primarily rely on census data, economic surveys, and predefined statistical units (e.g., census tracts or transportation analysis zones) to identify employment [16–19] or population subcenters [20, 21]. While recent efforts have incorporated mobile phone or social media data to improve center detection [22, 23], these data sources are often unavailable or inconsistent across countries, hindering global comparability. Recent initiatives, such as the European Union’s Urban Centre Database based on the Global Human Settlement

Layer (GHSL) [24], represent important progress in mapping urban cores worldwide. However, this database delineates entire agglomerations as single units rather than identifying the multiple activity centers nested within them. Consequently, the polycentric structures characteristic of modern metropolitan growth remain poorly captured by existing global representations or conventional proxies like population-weighted centroids [25, 26].

To address these limitations, we develop a geospatial framework that leverages nighttime light data (a well-established proxy for economic activity [27–31] and urban structure identification [32–34]) to construct a harmonized global map of intra-urban centers. In this study, a *city* refers to a contiguous urban agglomeration delineated by GHSL, independent of administrative boundaries, ensuring global consistency [35]. An *urban center* (or simply *center*) denotes a localized concentration of human activity within a city, operationally identified as a local maximum in nighttime light intensity. Analogous to mapping mountainous terrain, we treat nighttime light intensity as the “elevation” of urban activity and identify centers as local “peaks” in this landscape (Fig. 1).

Analyzing this global map reveals substantial diversity in the number and arrangement of centers across regions. Strikingly, beneath this heterogeneity lies a robust regularity: across more than 9,500 cities worldwide, the total urban area scales proportionally with the number of centers, a remarkably stable spatial footprint per center. At the level of individual centers, spatial catchment areas derived from Voronoi partitioning exhibit a characteristic size across countries, largely independent of population density. These regularities imply that as cities grow, they tend to accommodate expansion through the multi-

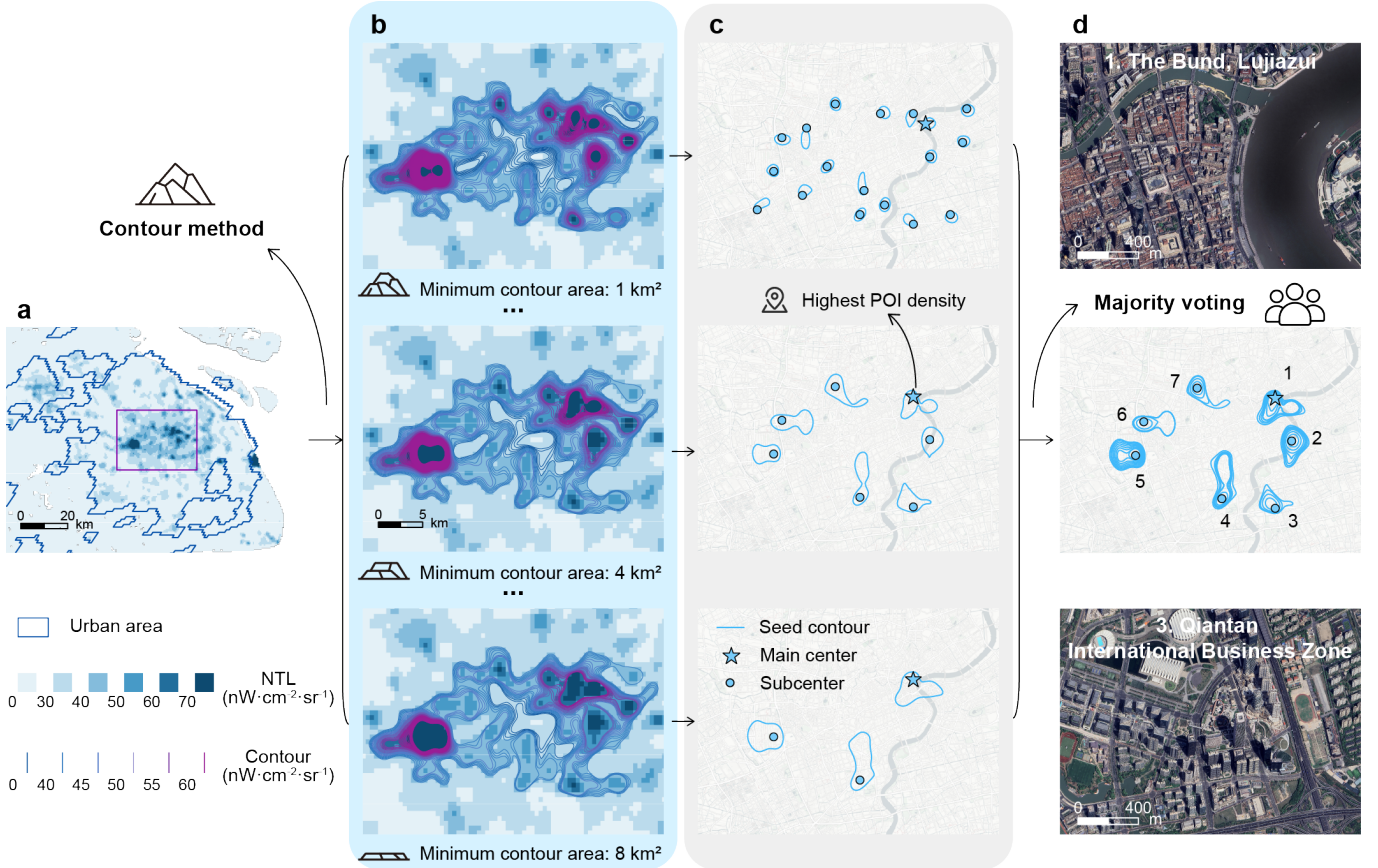


**Fig. 1. Scheme of the urban center identification methods.** (a) Nighttime light distribution around Shanghai, China. (b) Contour maps of the region under different minimum contour area values. (c) Centers under different minimum contour area values. The one with the highest POI density is labeled as the main center. (d) Majority voting across all minimum contour area values. The insets display close-up satellite views of the identified main center (top) and a subcenter (bottom). Imagery from Google.

plication of centers rather than the expansion of existing ones.

By identifying intra-urban activity centers in a globally consistent manner, this study provides a descriptive foundation for comparing internal urban structure across cities and regions. The resulting dataset enables systematic analyses of accessibility, spatial hierarchy, and center multiplicity using harmonized global data, and offers new empirical insights into the organizing principles of intra-urban spatial structure.

## RESULTS

### Identification of Intra-Urban Activity Centers

We briefly summarize the datasets and methodological framework here; detailed parameters, computation procedures, and validation analyses are provided in the Methods section and Extended Data Fig. 1.

Our analysis integrates five open-source datasets. The

primary inputs are the 2020 Global Human Settlement Layer Settlement Model (GHSL-SMOD) and the 2020 VIIRS nighttime light (NTL) data. From GHSL-SMOD, we extract urban areas classified as high-density clusters. Additional datasets are incorporated for characterization and evaluation, including Foursquare points-of-interest (POI) data, WorldPop population data, and GeoNames, which is used to assign standardized place names to identified centers.

Urban boundaries from GHSL-SMOD are used to mask the NTL data. We then apply a contour-based detection algorithm, adapted from the Localized Contour Tree Method ([33]), to identify intra-urban centers (Fig. 1). Nighttime light intensity is treated as a continuous surface reflecting spatial variation in human activity, and local intensity maxima serve as center candidates. To reduce sensitivity to regional differences in development levels and lighting practices, we avoid fixed brightness thresholds. Instead, centers are identified using an adaptive minimum coverage area criterion (Fig. 1b-c), which helps retain moderate-intensity local activity hubs that

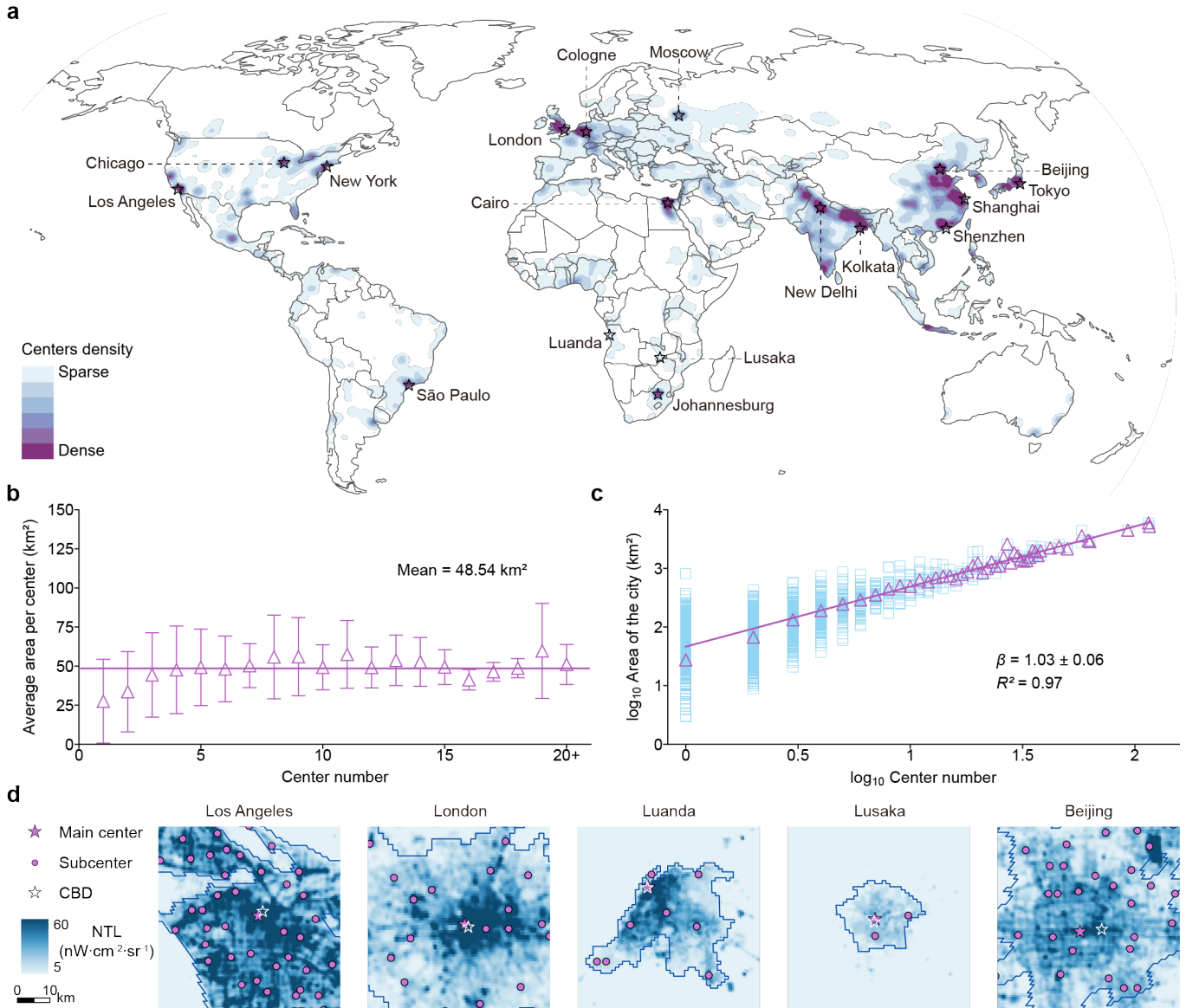


**Fig. 2. Geographic distribution of global urban centers.** (a) Heatmap of centers worldwide. Developed or densely populated regions typically have a high density of centers. (b) Average area per center relative to the center number of cities. Cities with  $\geq 20$  centers are aggregated. Triangles indicate the mean, error bars represent the standard deviation and the purple line denotes the average value of the means. (c) Scaling analysis between the total built-up area and center number. Squares represent individual cities, and triangles indicate group means. The line represents the fitting to the group means (triangles) of cities with more than one center ( $n = 46$ ) on a log-log scale. The scaling exponent  $\beta = 1.03$ . (d) The identified urban centers in Los Angeles, US; London, UK; Luanda, Angola; Lusaka, Zambia; and Beijing, China. Note that for simplicity, the extents of some cities are not fully depicted. The locations of the CBDs are collected from official government reports and online documents. The spatial proximity of the identified main centers (purple stars) to the CBDs (white stars) partially validates the accuracy of our center identification procedure.

might otherwise be excluded. Robustness is assessed through eight iterations with minimum coverage areas ranging from  $1 \text{ km}^2$  to  $8 \text{ km}^2$  (in  $1 \text{ km}^2$  intervals); a contour peak is retained as a center only if it appears in at least half of the iterations (Fig. 1d).

Center detection relies solely on nighttime light and urban boundary data. POI density and category composition are subsequently computed to characterize functional profiles and to label the primary center within each city. Centers are classified into seven functional types,

with mixed-use centers accounting for 61.2% of the total (Supplementary Fig. 1).

Validation is conducted through a stratified manual assessment of 1,000 centers worldwide. Each center is independently reviewed by urban and GIS experts using satellite imagery, OpenStreetMap, and other public sources, based on the presence of dense built-up morphology and recognizable commercial, governmental, or transportation facilities. Overall, 97.5% of the sampled centers satisfy these criteria, indicating strong spatial correspondence between detected centers and concentrated human activity. Representative misidentified cases, such as greenhouse complexes and highway interchanges, are shown in Supplementary Fig. 2.

Because identification relies on nighttime light intensity, not all GHSL-defined urban areas yield detectable centers. Approximately 17% of cities show no detectable activity centers, primarily due to either diffuse residential development with weak activity concentration or low-illumination contexts. These cases highlight known limitations of nighttime-light-based detection and motivate future integration of complementary data sources.

### Characteristics of Centers

Globally, we identify 15,834 activity centers across 9,582 cities. Their spatial distribution reflects both widespread urbanization and pronounced regional concentration (Fig. 2a). High density of centers are observed in large metropolitan regions, such as the eastern United States, central and west Europe, and eastern China. China hosts the largest number of detected centers (2,949), followed by India (2,146) and the United States (1,371), consistent with their large urban populations and extensive built-up areas. Within individual countries, however, centers are distributed unevenly. In China, 91.6% of centers are located east of the Heihe-Tengchong Line [36]—an area accounting for roughly one-third of the national territory. In India, approximately 40% of centers are located within the Indo-Gangetic Plain, which occupies about 20% of the country’s land area. In the United States, 67.6% of centers are concentrated in five census divisions that together account for only 28.1% of the national area.

Beyond this geographic heterogeneity, the number of centers varies substantially across cities, ranging from a single center to several dozen in large metropolitan areas. To examine how center abundance relates to urban scale, we analyze the relationship between the number of centers in each city and the average spatial area associated with each center, computed as the total GHSL urban area divided by the number of detected centers. Across all cities, the mean center area remains approximately constant as the number of centers increases (Fig. 2b), indicating that cities with more centers tend to subdivide

urban space rather than expand the spatial footprint of individual centers.

Consistent with this observation, scaling analysis further reveals a proportional relationship between the number of centers  $N_i$  of city  $i$  and the urban area  $A_i$  the city covers:

$$A_i = A_0 N_i^\beta \quad (1)$$

where  $\beta = 1.03$  (0.06) (Fig. 2c). This indicates a scale-invariant behavior: increases in the number of centers are accompanied by proportional increases in covered urban area, yielding a stable average area per center across cities of different sizes.

The high spatial resolution of the dataset further enables visualization of intra-urban center configurations. Figure 2d illustrates the spatial arrangement of detected centers in five representative cities—Los Angeles, London, Luanda, Lusaka, and Beijing (see also Extended Data Fig. 2)—highlighting substantial variation in center multiplicity and spatial dispersion. For example, Los Angeles exhibits a highly dispersed configuration with 93 detected centers, whereas London and Luanda display more compact patterns with 30 and 9 centers, respectively. Despite these differences in center number and spatial arrangement, the average spatial extent associated with each center remains comparable across cities, motivating a closer examination of how urban space is allocated among individual centers within cities.

### Stable Coverage Area of Centers Across Cities

The city-level scaling relationships described above characterize how urban space is partitioned across cities as they grow. However, such aggregate patterns do not reveal how space is allocated among individual centers within a city. In principle, a stable average area could mask substantial internal heterogeneity — for example, dominant central hubs surrounded by smaller peripheral centers, or compact inner-city centers coexisting with expansive suburban ones. We therefore examine whether the observed stability in center coverage also holds at the level of individual centers within cities.

We begin by analyzing the spatial partitioning induced by centers using Voronoi diagrams, which assign each location in a city to its nearest center. Figure 3a illustrates this construction for Los Angeles, where individual Voronoi polygons exhibit comparable areas despite substantial variation in center location and surrounding urban context (mean = 48 km<sup>2</sup>, SD = 20 km<sup>2</sup>). To assess whether this apparent regularity generalizes, we analyze Voronoi-based coverage areas across cities worldwide. Figure 3b shows kernel density estimates of total urban area for cities with one to five centers. While

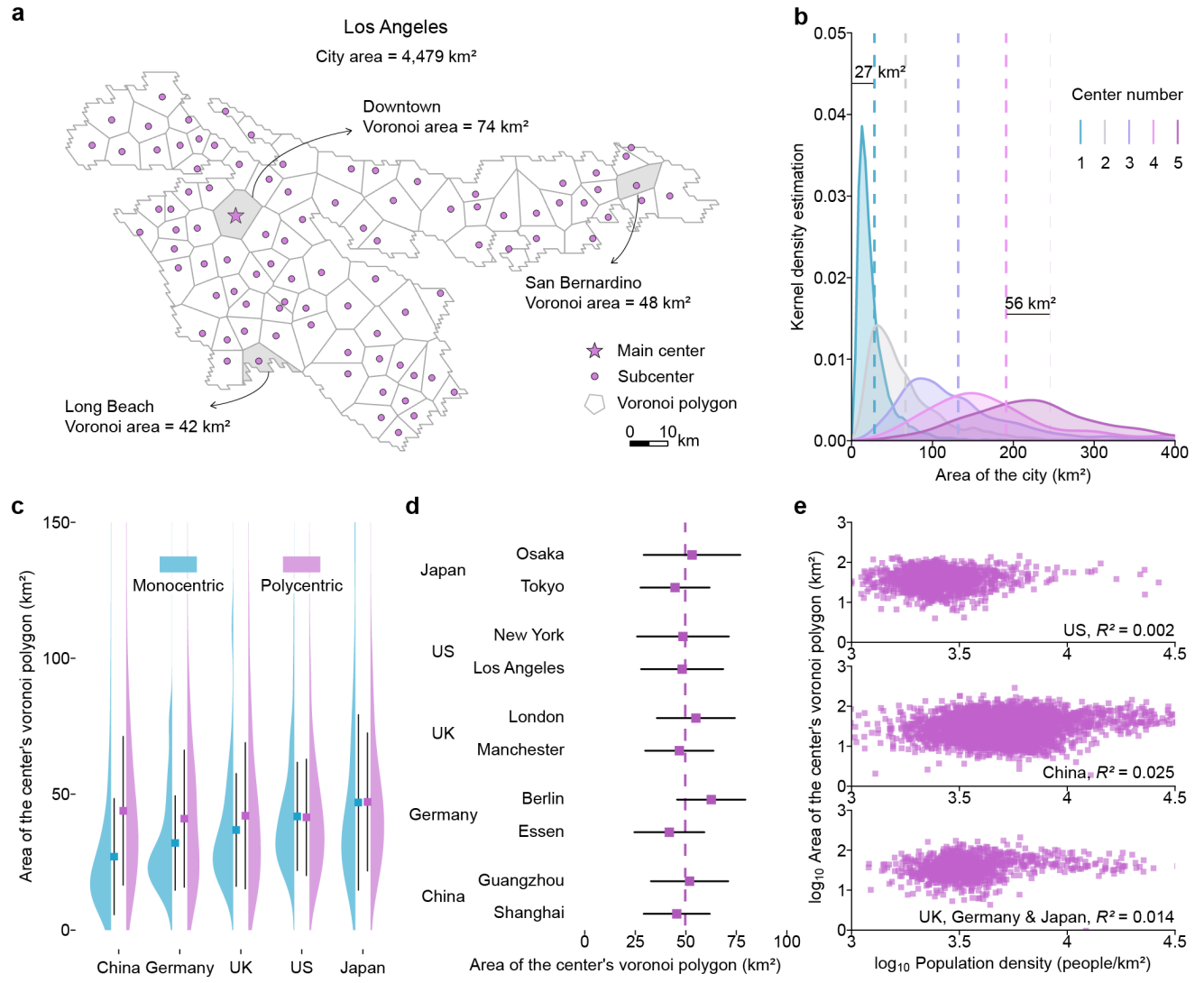


**Fig. 3. Spatial distribution of centers within the city.** (a) The Voronoi Diagram of centers in Los Angeles, US. (b) The kernel density estimation of the area distribution of cities with 1, 2, 3, 4, and 5 centers. The vertical dashed line represents the average area for each city group. The average area of monocentric cities, i.e., cities with a single center, is obviously smaller than the difference in average area between cities with consecutive numbers of centers. (c) Area distribution of centers' voronoi polygons in monocentric and polycentric cities for China, Germany, the UK, the US and Japan. The average coverage area of centers in polycentric cities remains stable across different countries. (d) Area distribution of centers' voronoi polygons in ten cities. Squares indicate the mean, error bars represent the standard deviation and the dashed purple line denotes the average value of the means. (e) The area versus population density of centers' voronoi polygons. The  $R^2$  values of the linear regression are rather small.

monocentric cities are substantially smaller on average, the incremental increase in urban area associated with each additional center remains nearly constant, yielding an average of approximately 50 km<sup>2</sup> per center.

This regularity is robust across countries and spatial scales. Figure 3c compares the distribution of Voronoi areas for centers in cities across China, Germany, the United Kingdom, the United States, and Japan, revealing a remarkably consistent mean coverage area —typically

between 41 and 47 km<sup>2</sup> per center —despite large differences in urban form, governance, and development context. Figure 3d further demonstrates that similar regularities hold within individual metropolitan areas, where centers with different functional roles and spatial positions nonetheless exhibit comparable coverage areas.

To ascertain whether the observed stability in center coverage reflects a deliberate spatial organizing principle rather than a statistical artifact of spatial partitioning,

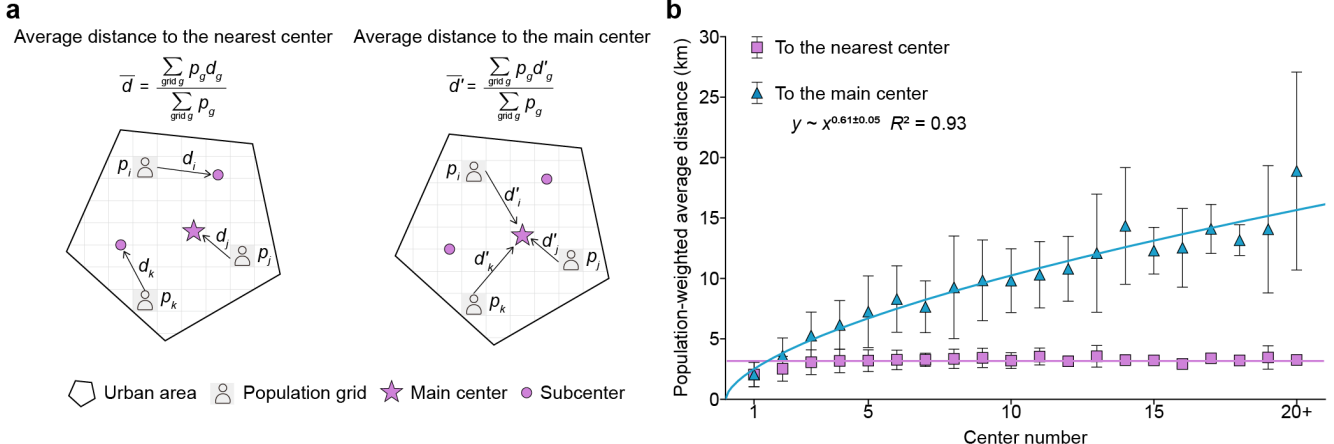


**Fig. 4. Population-weighted average distance to the center.** (a) Two types of average distance. For the average distance to the nearest center, we overlay the population grid on the urban area, calculate the distance to the nearest center of each grid, and average it by the population of grid. For the average distance to the main center, the distance to the main center of each grid is used. (b) Average distance relative to the center number of the urban area. Urban areas are grouped by the center number and those with at least 20 centers are grouped together. While the distance to the main center increases significantly with the number of centers, the distance to the nearest center remains stable. The scatters represent the mean and the error bars represent the standard deviation. The line for the main center represents the fitting to  $y = ax^b$ , and the line for the nearest center represents the average value of the means.

we compared the empirical distribution of Voronoi areas against a null model. In this model, we simulated a stochastic spatial process by randomly distributing the same number of "pseudo-centers" within the observed urban boundaries of each city. Our results show that the empirical Voronoi polygons exhibit a significantly lower coefficient of variation ( $CV_{emp} \approx 0.66$ ) compared to the null model ( $CV_{null} \approx 0.76$ ,  $p < 0.001$ ) for cities with at least 5 centers, indicating that real-world activity centers are far more regularly spaced than a random Poisson process would suggest. While random points frequently cluster or leave large spatial gaps — leading to highly skewed coverage areas — actual intra-urban centers appear to maintain a minimum exclusionary distance from one another. This self-organized repulsion ensures that each center commands a consistent spatial footprint, effectively tiling the urban fabric into functional cells of a characteristic scale.

We note that the absolute magnitude of this characteristic coverage area depends on how urban extent is delineated and on the underlying settlement or built-up datasets used. While the GHSL-based urban boundaries employed here yield an average center area on the order of  $50 \text{ km}^2$ , alternative representations of urban extent may lead to systematically different numerical values. Importantly, our primary finding concerns the scale-invariant relationship between urban area and center number, rather than the specific value of the characteristic area, which remains remarkably stable across cities within each dataset. Further evaluation using additional

global urban extent products will help refine the absolute magnitude of this characteristic scale.

To test whether this characteristic scale simply reflects variation in local population concentration, we examine the relationship between Voronoi area and population density at the level of individual centers. As shown in Fig. 3e, the association is weak across all examined regions, with  $R^2$  ranging from 0.002 in the United States to 0.025 in China, and 0.014 when pooling data from the United Kingdom, Germany, and Japan. These low correlations indicate that center coverage area is largely independent of local population density and nighttime light intensity, pointing to a robust spatial regularity rather than a direct demographic or intensity-driven effect.

This stabilization of coverage area has direct geometric implications for urban accessibility. As cities expand, the maintenance of a characteristic coverage area per center suggests a self-organizing mechanism that preserves local accessibility despite increasing urban scale. To quantify this, we compare the population-weighted mean distance to the nearest center under two scenarios: the observed polycentric configuration and a counterfactual monocentric baseline where all activity is consolidated into a single primary core (Fig. 4a).

As shown in Fig. 4b, we observe a striking divergence in accessibility trajectories as cities grow. Under the monocentric assumption, the average distance from the population to the main center increases monotonically and rapidly with the number of centers or built-up area following a power-law growth. For instance, in cities

where the number of centers doubles, the average distance to the main core increases by approximately 50%, significantly raising the time and energy costs of urban interaction. In sharp contrast, the empirical distance to the nearest center remains remarkably invariant, fluctuating around a stable baseline regardless of whether a city possesses two or twenty centers.

This stability indicates that the emergence of new activity centers serves as a spatial adaptation to growth. By replicating the consistent footprint, cities effectively “tile” the landscape with accessible hubs, ensuring that the average resident’s proximity to essential urban services is decoupled from the overall size of the metropolitan area. This accessibility-preserving multiplication suggests that the  $50 \text{ km}^2$  scale may represent a functional equilibrium: it is large enough to foster agglomeration economies yet small enough to keep daily destinations within a manageable travel radius, likely constrained by universal limits on human travel time budgets.

Importantly, this contrast is robust to alternative population datasets and to variations in center detection parameters (Extended Data Fig. 3), confirming that it reflects a fundamental geometric property of polycentric organization rather than a data-specific artifact.

## DISCUSSION

By constructing a globally consistent dataset of intra-urban activity centers, this study reveals both the diversity of contemporary urban spatial organization and a striking regularity underlying that diversity. Across more than 9,500 cities worldwide, we find that despite large variation in city size, center multiplicity, and regional context, the spatial coverage associated with individual centers remains remarkably stable. This scale-invariant pattern holds both at the city level — where total urban area scales proportionally with the number of centers — and within cities, where individual centers exhibit comparable coverage areas regardless of location, functional role, or surrounding population density. Together, these findings suggest that polycentric configurations are not merely the idiosyncratic outcomes of local planning, but emerge as a generic spatial response to urban growth.

This regularity complements and extends the literature on urban scaling laws [2, 37], which has documented systematic power-law relationships between city size and aggregate socioeconomic outputs. While most prior work has focused on macroscopic properties of cities treated as single units, our results point to an analogous scaling principle operating at the intra-urban scale: as cities expand, urban space is subdivided into a growing number of activity centers, each associated with a characteristic spatial extent. In this sense, the observed stability of the spatial unit per center acts as a fundamental building block that ensures the internal fabric of the city remains

functional as the system scales.

Beyond identifying centers, our dataset enables a more nuanced characterization of urban spatial structure [9, 38–40]. A prominent example is the spatial decay of population density from urban centers toward peripheral areas. Traditional studies of density gradients have largely assumed monocentric urban structure, estimating decay functions with respect to a single city center. By contrast, our polycentric center data allow population density to be examined relative to both main centers and subcenters. As illustrated in Fig. 5, population density generally decays more steeply around primary centers than around secondary centers, revealing systematic differences in agglomeration intensity that are obscured under monocentric assumptions. These results demonstrate how explicitly accounting for multiple centers can refine empirical characterizations of urban form and provide a more nuanced basis for testing urban theories.

Despite these advances, several limitations remain. A key constraint lies in using nighttime light intensity as a proxy for urban activity, which may not fully capture urban vibrancy across all contexts [41, 42]. Although our method can identify centers in dim-lit regions when sufficient NTL variation exists (Extended Data Fig. 4), geographic and cultural biases in NTL data compromise global consistency. Cities with energy-saving policies, irregular electricity supply, or weak nighttime illumination may be under-identified, while brightly lit non-urban features — such as greenhouse complexes or highway interchanges — may occasionally be misclassified as centers. Although manual validation and robustness analyses indicate that such cases are relatively rare, addressing them will require integrating complementary data sources, including road networks, daytime remote-sensing imagery, and supervised learning approaches. At the same time, assembling globally representative training data with consistent semantic labels remains a significant challenge.

Another constraint concerns the lack of comparable datasets for intra-urban centers. To partially validate our results, we compiled planning documents from Seattle, Portland, Beijing, and London, which explicitly designate government-identified urban centers. We georeferenced these centers in GIS and compared them with our detected results. Overall, 30 of the 34 planned centers across the four cities were successfully identified by our method (Extended Data Fig. 5).

Finally, future research should explore linking the identified centers with direct observations of human mobility [43–46]. Specifically, the emergence of a characteristic coverage area per center is consistent with previously reported regularities in human movement and visitation behavior[47]. Empirical work on visitation laws has shown that interaction volumes between locations decay sharply with both distance and visit frequency, leading to well-defined spatial catchments under minimum fre-

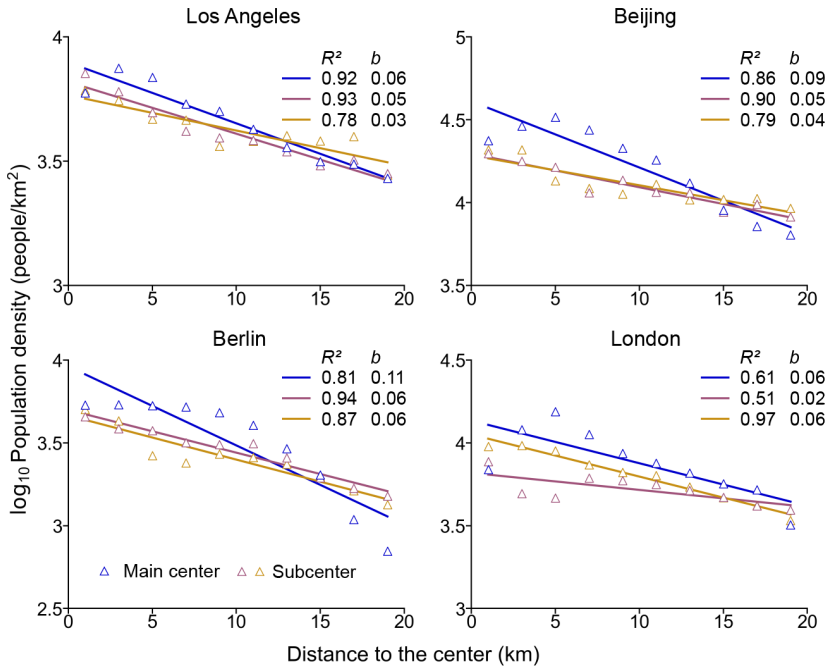


**Fig. 5. Population density decay from urban center to peripheries.** Scatter plots show population density distributions around the main and sub-centers for Los Angeles (US); Beijing (China); Berlin (Germany); and London (UK). Each point represents the average population density within a 2-km-wide concentric ring. Lines represent the linear regression fits to  $\log y = \log a + bx$ . Generally, density decays more steeply around main urban centers than subcenters, as indicated by the larger decay coefficients  $b$ .

frequency or flow constraints. Similarly, the Marchetti constant — the empirical regularity that individuals across societies devote a roughly constant amount of daily time to travel — imposes an upper bound on the spatial reach of routine activities [46]. Together, these behavioral constraints provide a plausible micro-scale interpretation for why urban activity centers across diverse contexts are associated with similar spatial extents. Directly testing these mechanisms will require integrating center locations with high-resolution mobility data in future work.

## METHODS

### Data

We integrated five primary datasets: Global Human Settlement Layer – Settlement Model (GHSL-SMOD) [48], nighttime light data from the Visible Infrared Imaging Radiometer Suite (NPP-VIIRS NTL) [49], Foursquare Open Source (FSQ OS) Places [50], GeoNames geographical database [51], and WorldPop Population Counts [52]. GHSL-SMOD provides the spatial extent of cities; NPP-VIIRS NTL provide a proxy for aggregated human activity used to identify intra-urban centers; FSQ OS Places support center labeling and functional characterization; GeoNames supplies standardized

place names; and WorldPop provides population estimates for regional comparisons and accessibility analyses.

GHSL-SMOD delineates global settlements based on population size, population density, and built-up area, following the Degree of Urbanisation framework [53]. We selected the 2020 high density cluster, defined as contiguous 1  $\text{km}^2$  grid cells with at least 1,500 people per  $\text{km}^2$  or over 50% built-up area, and a minimum population of 50,000.

The VIIRS Day/Night Band (DNB) measures radiance in units of  $\text{nW} \cdot \text{cm}^{-2} \cdot \text{sr}^{-1}$  with a spatial resolution of  $\sim 500$  m. We used the 2020 annual composite (version “vcmslcfg”), which filters out transient light sources such as sunlight, moonlight, biomass burning, and aurora [49]. Background noise was removed by setting low-intensity values to zero using a standard brightness threshold.

FSQ OS Places provides global points of interest across 1,245 categories, including business, government, retail, dining, and transportation. GeoNames integrates multi-source geographic information, including place names and administrative units. WorldPop offers global population mosaics at 1-km resolution derived from top-down models calibrated to national census data; we used the 2020 unconstrained product.

All datasets were projected to the WGS84 coordinate system. Urban areas were calculated geodesically, and

population and brightness were aggregated within GHSL-SMOD boundaries using spatial masking.

### Contour Methods to Identify Local Activity Centers

We identified intra-urban activity centers using a modified Localized Contour Tree method [33]. In this framework, nighttime light intensity is conceptualized as a continuous surface of aggregated human activity, with local maxima representing candidate centers. Because contour extraction requires spatially smoothed input data, we followed established practice and applied a Gaussian filter ( $3 \times 3$  pixels,  $\sigma = 5$ ) to the nighttime light imagery to enhance spatial continuity and eliminate ill-formed contours [33]. Contours were extracted at  $1 \text{ nW} \cdot \text{cm}^{-2} \cdot \text{sr}^{-1}$  intervals within each GHSL-defined urban boundary. Higher-intensity contours enclose progressively smaller areas, analogous to elevation contours in topographic analysis.

To distinguish meaningful centers from minor intensity variations, we introduced a minimum contour area threshold—the main tuning parameter of the approach—which defines the smallest spatial extent considered representative of a localized activity concentration. As illustrated in Fig. 1b, a contour is considered a valid peak contour if it satisfies two conditions: (i) it does not contain any smaller contour that also meets the area criterion (i.e., no nested qualified contour exists within it), and (ii) its NTL value is higher than that of surrounding contours, ensuring it represents a local maximum rather than a saddle or valley. For each retained contour, the brightest pixel is selected as the representative center location.

To assess robustness to parameter choice, we repeated the detection process using eight minimum area thresholds ranging from 1 to  $8 \text{ km}^2$  (in  $1 \text{ km}^2$  increments), covering typical spatial scales of intra-urban centers. A candidate center was retained if it was identified in at least four of the eight runs (majority voting). The vote count also serves as a confidence measure: more than two-thirds of the retained centers were consistently identified under all parameter settings (Supplementary Fig. S3).

Because detection relies on nighttime light intensity within GHSL-defined urban extents, not all urban areas yield detectable centers. In total, 1,951 cities (17%, Extended Data Fig. 6) exhibit no detectable activity centers. These cases arise for two primary reasons. First, some densely populated settlements—mainly in Nigeria, China and India—meet GHSL criteria for population density and built-up area but display diffuse nighttime light patterns without pronounced local maxima. In such cases, residential clustering is evident, yet neither nighttime lights nor high-resolution daytime imagery reveal localized concentrations of activity (Extended Data Fig.

7a–c). Second, cities in low-illumination contexts, such as Pyongsong (North Korea), exhibit clearly defined urban cores in satellite imagery but insufficient nocturnal lighting for reliable detection (Extended Data Fig. 7d). These limitations motivate future integration of complementary data sources, such as multispectral imagery, to improve coverage in low-light environments.

### Attribute Enhancement

Beyond center identification, we enriched the dataset by labeling main centers, assigning place names, and characterizing functional types.

First, we classified main centers and subcenters. In monocentric cities, the single detected center was designated as the main center. In polycentric cities, we calculated POI density within each center’s contour; the center with the highest POI density was labeled the main center, and all others were classified as subcenters.

Second, each center was assigned a place name and a functional category. Place names were obtained by matching centers to the nearest GeoNames record within a 1-km buffer. Functional classification was based on POIs aggregated within the same buffer and grouped into six major categories: Mixed, Consumption, Business, Public Service, Transport, and Industrial. We calculated the Shannon entropy  $H = -\sum_{i=1}^5 p_i \log p_i$  to quantify category diversity. Centers with  $H > 1.5$  were labeled as Mixed; otherwise, centers were assigned the dominant POI category. Mixed-use centers account for 61.2% of all detected centers, consistent with independent land-use comparisons (Extended Data Fig. 8; Supplementary Fig. S1).

Finally, although the brightest pixel within each contour provides a consistent proxy for center location, it may occasionally align with peripheral bright facilities such as stadiums or logistics hubs. To address this, we manually reviewed and refined the locations of main centers using satellite imagery and OpenStreetMap. In total, 5,444 urban areas (57%) were inspected, resulting in a refinement rate of 19.8% and a median adjustment distance of 2.3 km. Importantly, both the original automatically detected center coordinates and the refined coordinates are provided in the public dataset. All statistical analyses reported in this study—including scaling relationships, Voronoi-based coverage areas, and accessibility metrics—are unaffected by this post-processing refinement, which is intended solely to enhance usability in applied contexts.

Because activity centers represent spatial extents rather than point locations, we provide the full contour geometries alongside point coordinates in the public dataset to support future spatial and comparative analyses.

## Acknowledgment

We thank the support of the National Key Research and Development Program of China (Grant No. 2023YFB3906801), the National Natural Science Foundation of China (Grant No. 42422110), the Fundamental Research Funds for the Central Universities, Peking University. P.S. thanks the support by the Beijing Key Lab of Spatial Information Integration and Its Applications, Peking University.

## Author contributions

L.D. conceived the project; S.P. collected the data; S.P., J.Z., Y.L., and L.D. analyzed the data; L.D., S.P., and Y.L. wrote the manuscript.

## Data availability

The data used in this paper are publicly available; the nighttime light data can be downloaded from <https://eogdata.mines.edu/products/vnl/>, the urban area data can be downloaded from (<https://human-settlement.emergency.copernicus.eu/download.php>), the population data can be downloaded from Worldpop (<https://www.worldpop.org/>), the POI data can be downloaded from Foursquare OS (<https://opensource.foursquare.com/os-places/>), and the geonames data can be downloaded from GeoNames (<https://www.geonames.org/>).

## Code availability

All analyses were performed in Python. The code developed for the analysis is available via GitHub at <https://github.com/urbansci/city-centers>.

## Competing interests

The authors declare no competing interests.

---

- [1] Xiaoping Liu, Yinghui Huang, Xiaocong Xu, Xuecao Li, Xia Li, Philippe Ciais, Peirong Lin, Kai Gong, Alan D Ziegler, Anping Chen, et al. High-spatiotemporal-resolution mapping of global urban change from 1985 to 2015. *Nature Sustainability*, 3(7):564–570, 2020.
- [2] Luís MA Bettencourt, José Lobo, Dirk Helbing, Christian Kühnert, and Geoffrey B West. Growth, innovation, scaling, and the pace of life in cities. *Proceedings of the National Academy of Sciences*, 104(17):7301–7306, 2007.

- [3] Edward Glaeser. *Triumph of the City*. Penguin, 2012.
- [4] Karen C Seto, Shobhakar Dhakal, Anthony Bigio, Hilda Blanco, Gian Carlo Delgado, David Dewar, Luxin Huang, Atsushi Inaba, Arun Kansal, Shuaib Lwasa, et al. *Human Settlements, Infrastructure, and Spatial Planning*. Cambridge University Press, 2014.
- [5] Masahisa Fujita and Jacques-François Thisse. Economics of agglomeration. *Journal of the Japanese and International Economies*, 10(4):339–378, 1996.
- [6] Edward Glaeser. Cities, productivity, and quality of life. *Science*, 333(6042):592–594, 2011.
- [7] Alain Bertaud. *Order without Design: How Markets Shape Cities*. MIT Press, 2018.
- [8] Colin Clark. Urban population densities. *Journal of the Royal Statistical Society. Series A (General)*, 114(4):490–496, 1951.
- [9] Alex Anas, Richard Arnott, and Kenneth A Small. Urban spatial structure. *Journal of Economic Literature*, 36(3):1426–1464, 1998.
- [10] Charlotte Liotta, Vincent Viguié, and Quentin Lepetit. Testing the monocentric standard urban model in a global sample of cities. *Regional Science and Urban Economics*, 97:103832, 2022.
- [11] Siqi Zheng and Matthew E Kahn. Land and residential property markets in a booming economy: New evidence from beijing. *Journal of Urban Economics*, 63(2):743–757, 2008.
- [12] Rémi Louf and Marc Barthelemy. Modeling the polycentric transition of cities. *Physical Review Letters*, 111:198702, 11 2013.
- [13] D J Weiss, Andy Nelson, HS Gibson, W Temperley, Stephen Peedell, Allie Lieber, Matt Hancher, Eduardo Poyart, Simão Belchior, Nancy Fullman, et al. A global map of travel time to cities to assess inequalities in accessibility in 2015. *Nature*, 553(7688):333–336, 2018.
- [14] Andrea Cattaneo, Andrew Nelson, and Theresa McMenomy. Global mapping of urban–rural catchment areas reveals unequal access to services. *Proceedings of the National Academy of Sciences*, 118(2):e2011990118, 2021.
- [15] Andrea Cattaneo, Serkan Girgin, Rolf de By, Theresa McMenomy, Andrew Nelson, and Sara Vaz. Worldwide delineation of multi-tier city-regions. *Nature Cities*, 1(7):469–479, 2024.
- [16] Daniel A Griffith. Evaluating the transformation from a monocentric to a polycentric city. *The Professional Geographer*, 33(2):189–196, 1981.
- [17] John F McDonald. The identification of urban employment subcenters. *Journal of Urban Economics*, 21(2):242–258, 1987.
- [18] Daniel P McMillen. Nonparametric employment subcenter identification. *Journal of Urban Economics*, 50(3):448–473, 2001.
- [19] Christian L Redfearn. The topography of metropolitan employment: Identifying centers of employment in a polycentric urban area. *Journal of Urban Economics*, 61(3):519–541, 2007.
- [20] Yingcheng Li. Towards concentration and decentralization: The evolution of urban spatial structure of chinese cities, 2001–2016. *Computers, Environment and Urban Systems*, 80:101425, 2020.
- [21] Francesca Mariani, Ilaria Zambon, and Luca Salvati. Population matters: Identifying metropolitan subcenters from diachronic density-distance curves, 1960–

2010. *Sustainability*, 10(12):4653, 2018.

[22] Jixuan Cai, Bo Huang, and Yimeng Song. Using multi-source geospatial big data to identify the structure of polycentric cities. *Remote Sensing of Environment*, 202:210–221, 2017.

[23] Longxu Yan, Yishu Wang, De Wang, Shangwu Zhang, and Yang Xiao. A new approach for identifying urban employment centers using mobile phone data: A case study of Shanghai. *International Journal of Geographical Information Science*, 37(5):1180–1207, 2023.

[24] I. Mari Rivero, M. Melchorri, P. Florio, M. Schiavina, K. Krasnodebska, P. Politis, J. Uhl, M. Pesaresi, L. Maffenini, P. Sulis, M. Crippa, D. Guizzardi, E. Pisoni, C. Belis, D. Oom, A. Branco, D. Mwaniki, E. Kochulem, D. Githira, A. Carioli, D. Ehrlich, P. Tommasi, K. Thomas, and D. Lewis. *GHS Urban Centre Database 2024, multitemporal and multidimensional attributes, R2024A*. European Commission, Joint Research Centre (JRC), 2024.

[25] Niclas Lavesson. How does distance to urban centres influence necessity and opportunity-based firm start-ups? *Papers in Regional Science*, 97(4):1279–1304, 2018.

[26] Tomoya Mori, Tony E Smith, and Wen-Tai Hsu. Common power laws for cities and spatial fractal structures. *Proceedings of the National Academy of Sciences*, 117(12):6469–6475, 2020.

[27] Dave Donaldson and Adam Storeygard. The view from above: Applications of satellite data in economics. *Journal of Economic Perspectives*, 30(4):171–198, 2016.

[28] Marshall Burke, Anne Driscoll, David B Lobell, and Stefano Ermon. Using satellite imagery to understand and promote sustainable development. *Science*, 371(6535):eabe8628, 2021.

[29] Xi Chen and William D Nordhaus. Using luminosity data as a proxy for economic statistics. *Proceedings of the National Academy of Sciences*, 108(21):8589–8594, 2011.

[30] J Vernon Henderson, Adam Storeygard, and David N Weil. Measuring economic growth from outer space. *American economic review*, 102(2):994–1028, 2012.

[31] Jiandong Chen, Ming Gao, Shulei Cheng, Wenxuan Hou, Malin Song, Xin Liu, and Yu Liu. Global 1 km × 1 km gridded revised real gross domestic product and electricity consumption during 1992–2019 based on calibrated nighttime light data. *Scientific Data*, 9(1):202, 2022.

[32] Zhiwei Yang, Yingbiao Chen, Guanhua Guo, Zihao Zheng, and Zhifeng Wu. Using nighttime light data to identify the structure of polycentric cities and evaluate urban centers. *Science of the Total Environment*, 780:146586, 2021.

[33] Zuoqi Chen, Bailang Yu, Wei Song, Hongxing Liu, Qusheng Wu, Kaifang Shi, and Jianping Wu. A new approach for detecting urban centers and their spatial structure with nighttime light remote sensing. *IEEE Transactions on Geoscience and Remote Sensing*, 55(11):6305–6319, 2017.

[34] Na Jie, Xin Cao, and Li Zhuo. Identifying the Central Business Districts of global megacities using nighttime light remote sensing data. *International Journal of Digital Earth*, 17(1):2356118, 2024.

[35] Lei Dong, Fabio Duarte, Gilles Duranton, Paolo Santi, Marc Barthélémy, Michael Batty, Luís Bettencourt, Michael Goodchild, Gary Hack, Yu Liu, et al. Defining a city—delineating urban areas using cell-phone data. *Nature Cities*, 1(2):117–125, 2024.

[36] Huanyong Hu. The distribution of population in China. *Acta Geographica Sinica*, 2(2):33–74, 1983.

[37] Fabiano L Ribeiro and Diego Rybski. Mathematical models to explain the origin of urban scaling laws. *Physics Reports*, 1012:1–39, 2023.

[38] Daniel P McMillen and Stefani C Smith. The number of subcenters in large urban areas. *Journal of Urban Economics*, 53(3):321–338, 2003.

[39] Gilles Duranton and Diego Puga. Urban land use. In *Handbook of Regional and Urban Economics*, volume 5, pages 467–560. Elsevier, 2015.

[40] Masahisa Fujita, Paul R Krugman, and Anthony Venables. *The Spatial Economy: Cities, Regions, and International Trade*. MIT Press, 2001.

[41] Richard Bluhm and Melanie Krause. Top lights: Bright cities and their contribution to economic development. *Journal of Development Economics*, 157:102880, 2022.

[42] Chao Wu, Minwei Zhao, and Yu Ye. Measuring urban nighttime vitality and its relationship with urban spatial structure: A data-driven approach. *Environment and Planning B: Urban Analytics and City Science*, 50(1):130–145, 2023.

[43] Thomas Louail, Maxime Lenormand, Oliva G Cantu Ros, Miguel Picornell, Ricardo Herranz, Enrique Frias-Martinez, José J Ramasco, and Marc Barthélémy. From mobile phone data to the spatial structure of cities. *Scientific Reports*, 4(1):5276, 2014.

[44] Mattia Mazzoli, Alex Molas, Aleix Bassolas, Maxime Lenormand, Pere Colet, and José J Ramasco. Field theory for recurrent mobility. *Nature Communications*, 10(1):3895, 2019.

[45] Aleix Bassolas, Hugo Barbosa-Filho, Brian Dickinson, Xerxes Dotiwalla, Paul Eastham, Riccardo Gallotti, Gourab Ghoshal, Bryant Gipson, Surendra A Hazarie, Henry Kautz, et al. Hierarchical organization of urban mobility and its connection with city livability. *Nature Communications*, 10(1):4817, 2019.

[46] Lei Dong, Paolo Santi, Yu Liu, Siqi Zheng, and Carlo Ratti. The universality in urban commuting across and within cities. *arXiv preprint arXiv:2204.12865*, 2022.

[47] Markus Schläpfer, Lei Dong, Kevin O’Keeffe, Paolo Santi, Michael Szell, Hadrien Salat, Samuel Anklesaria, Mohammad Vazifeh, Carlo Ratti, and Geoffrey B West. The universal visitation law of human mobility. *Nature*, 593(7860):522–527, 2021.

[48] M Schiavina, M Melchorri, and M Pesaresi. GHS-SMOD R2023A - GHS settlement layers, application of the degree of urbanisation methodology (stage i) to GHS-POP R2023A and GHS-BUILT-S R2023A, multitemporal (1975–2030), 2023.

[49] Christopher D Elvidge, Mikhail Zhizhin, Tilottama Ghosh, Feng-Chi Hsu, and Jay Taneja. Annual time series of global VIIRS nighttime lights derived from monthly averages: 2012 to 2019. *Remote Sensing*, 13(5):922, 2021.

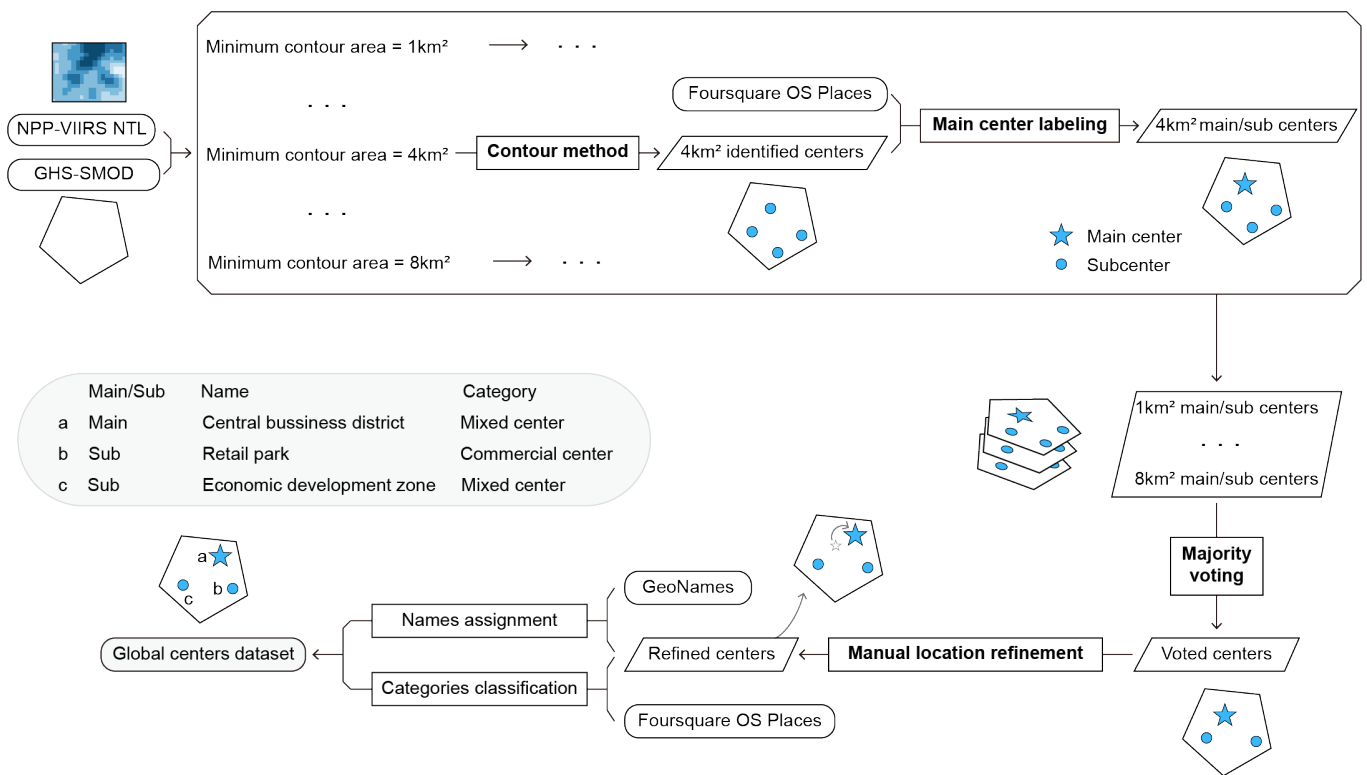
[50] Foursquare. Foursquare Open Source Places. <https://opensource.foursquare.com/os-places/>. Accessed: 2025-07-11.

[51] GeoNames. GeoNames Geographical Database. <https://www.geonames.org>. Accessed: 2024-03-01.

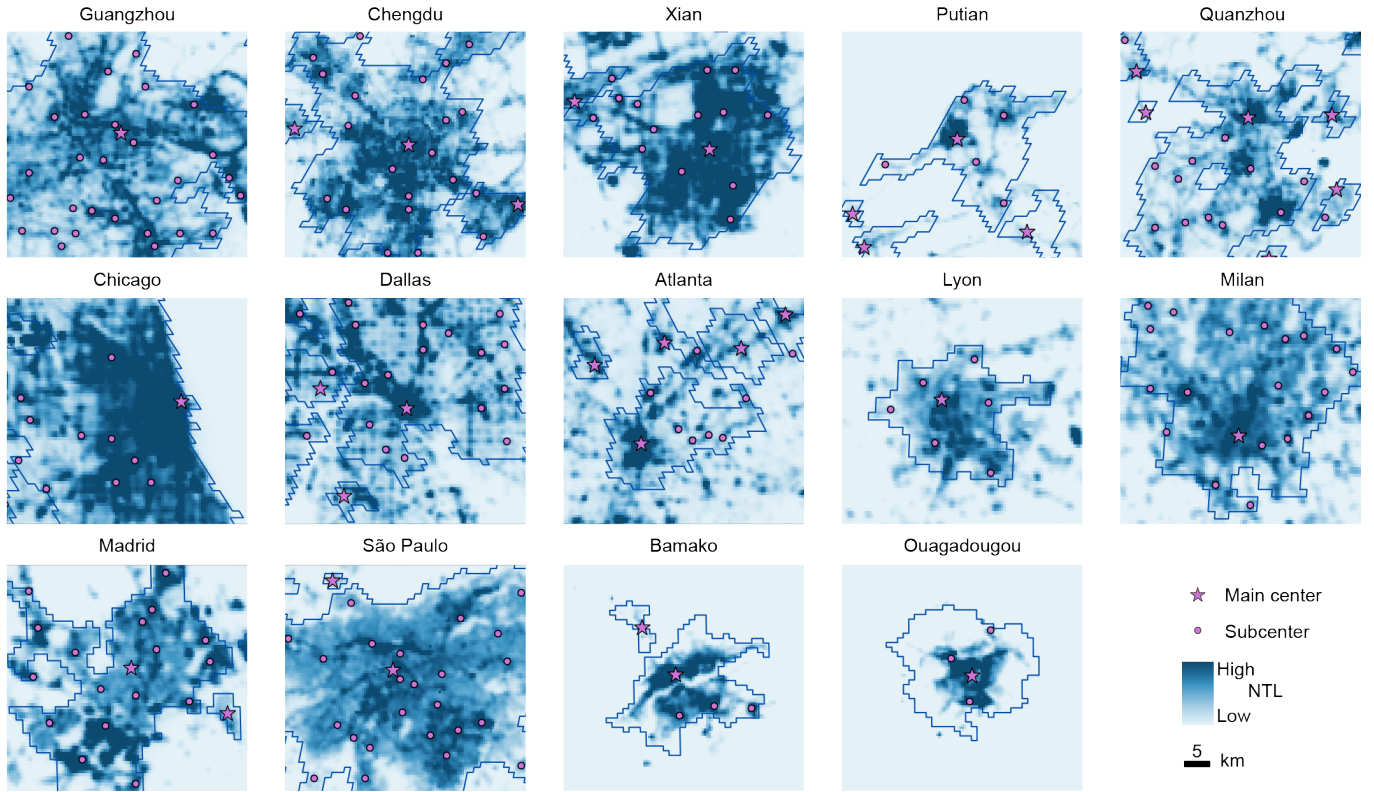
[52] M. Bondarenko, R. Priyatikanto, N. Tejedor-Garavito, W. Zhang, T. McKeen, A. Cunningham, T. Woods, J. Hilton, D. Cihan, B. Nosatiuk, T. Brinkhoff, A. Tatem, and A. Sorichetta. The spatial distribution of popu-

lation in 2015–2030 at a resolution of 30 arc (approximately 1 km at the equator) r2025a version v1. Global Demographic Data Project - Funded by The Bill and Melinda Gates Foundation (INV-045237). WorldPop - School of Geography and Environmental Science, University of Southampton, 2025. Accessed: 2025-10-11.

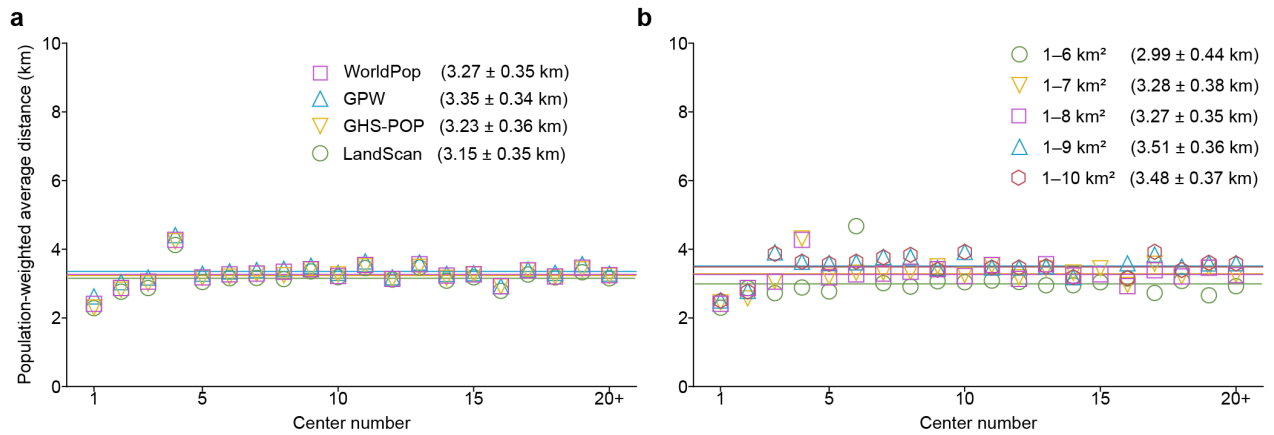
[53] European Commission and Eurostat. *Applying the degree of urbanisation – A methodological manual to define cities, towns and rural areas for international comparisons – 2021 edition*. Publications Office of the European Union, 2021.



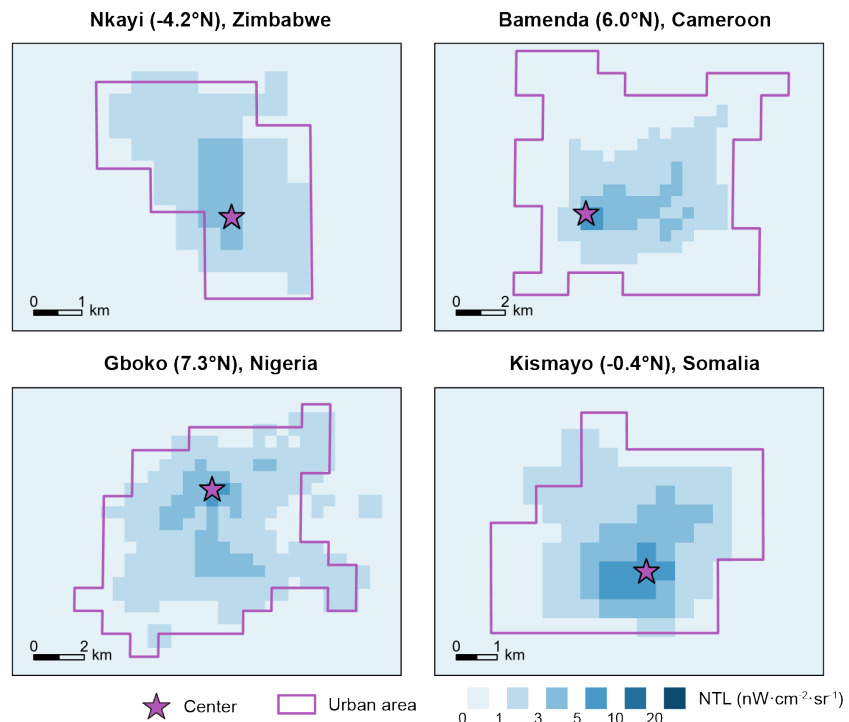
**Extended Data Figure 1.** Workflow of the study. Rounded rectangles denote input and output datasets; rectangles denote methods; and parallelograms denote intermediate data. The key methods are highlighted in bold.



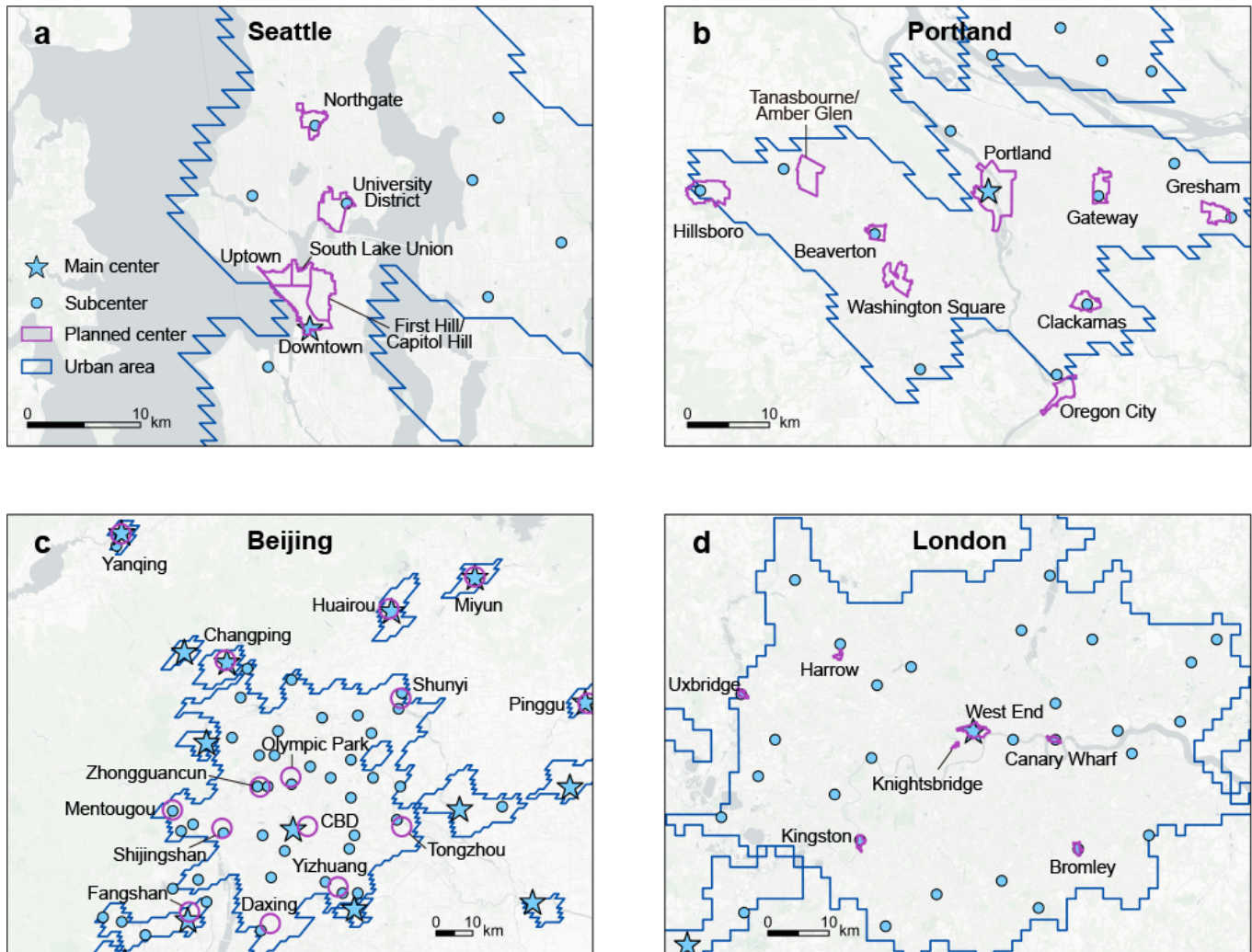
**Extended Data Figure 2.** Identified urban centers in representative cities. Guangzhou, Chengdu, Xi'an, Putian, and Quanzhou (China); Chicago, Dallas, and Atlanta (United States); Lyon (France); Milan (Italy); Madrid (Spain); São Paulo (Brazil); Bamako (Mali); and Ouagadougou (Burkina Faso).



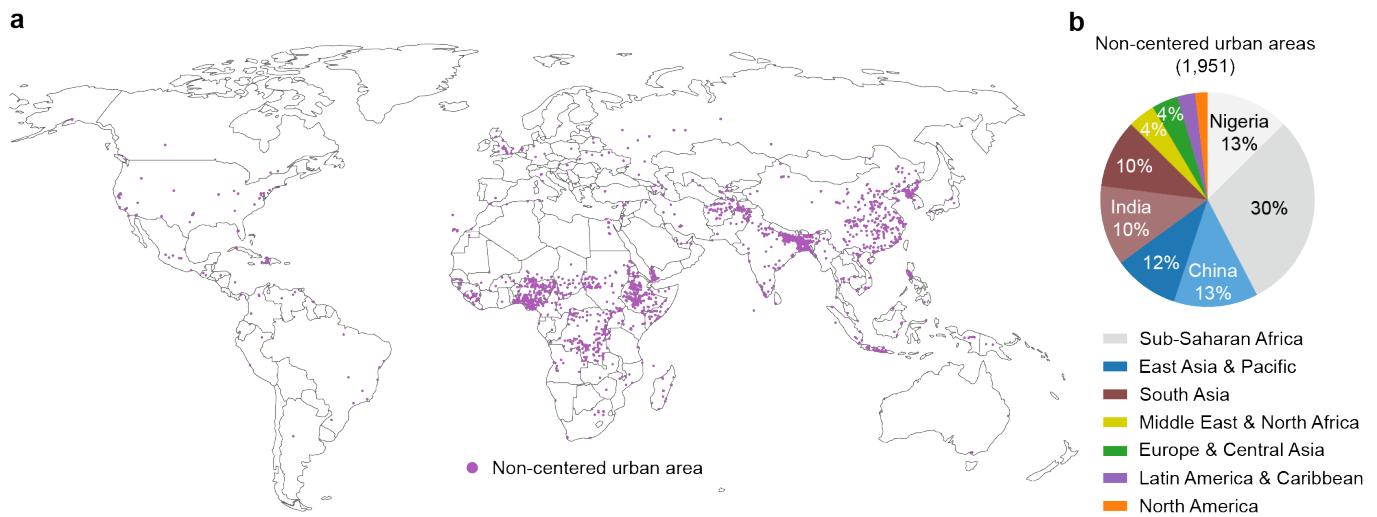
**Extended Data Figure 3.** Robustness check of the stabilization of the average distance to the nearest center across cities. The relationship between population-weighted average distance and center count remains consistent when varying (a) the population source data (under default 1–8 parameter setting) and (b) the contour parameter thresholds (using WorldPop). Cities are grouped by the center number and those with at least 20 centers are grouped together. Scatters denote the mean and values in parentheses represent the average value and standard deviation of means.



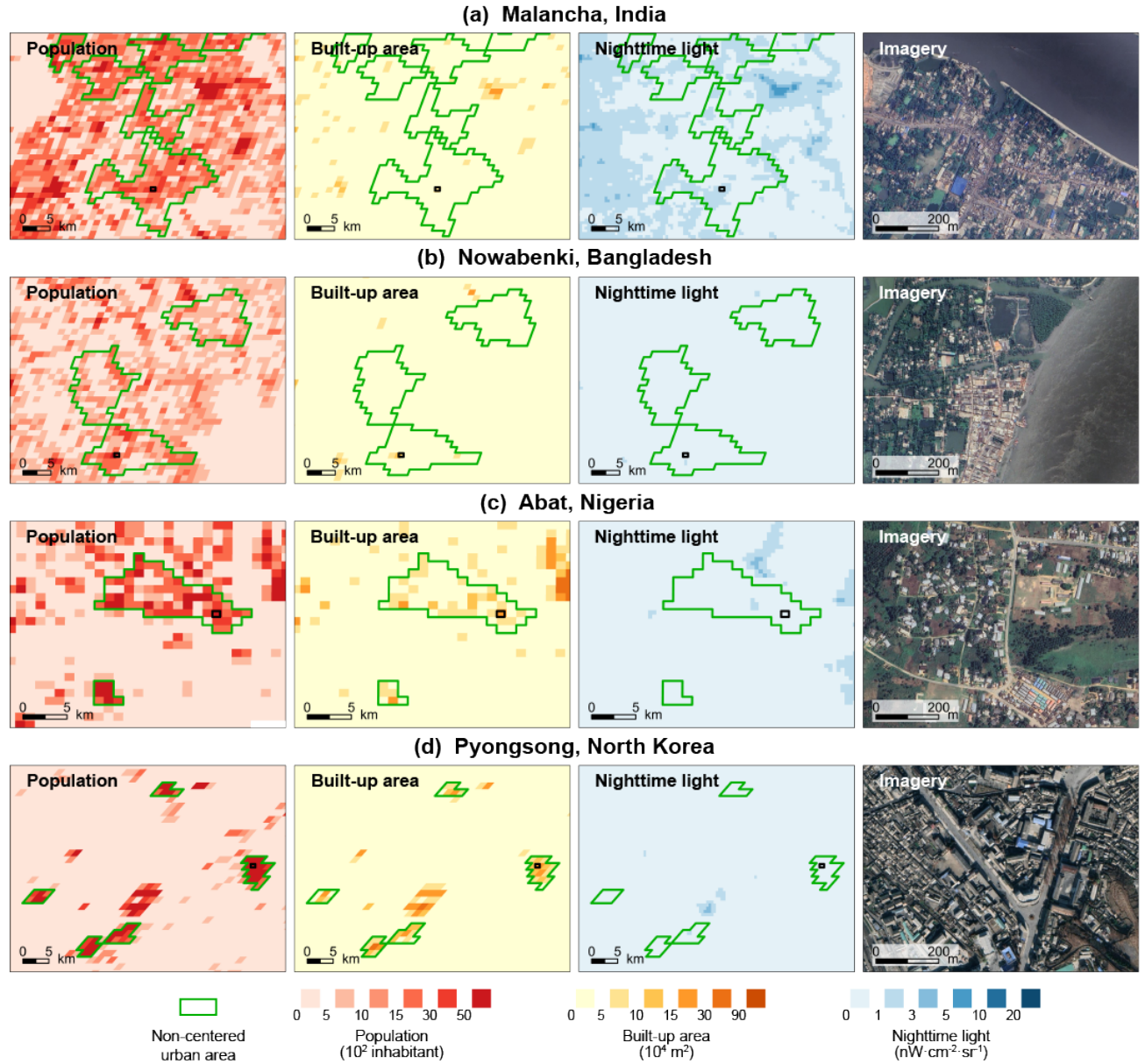
**Extended Data Figure 4.** Urban centers identification in tropical cities. Center can be identified if its surrounding area is significantly brighter than nearby regions, even if the overall city brightness is low.



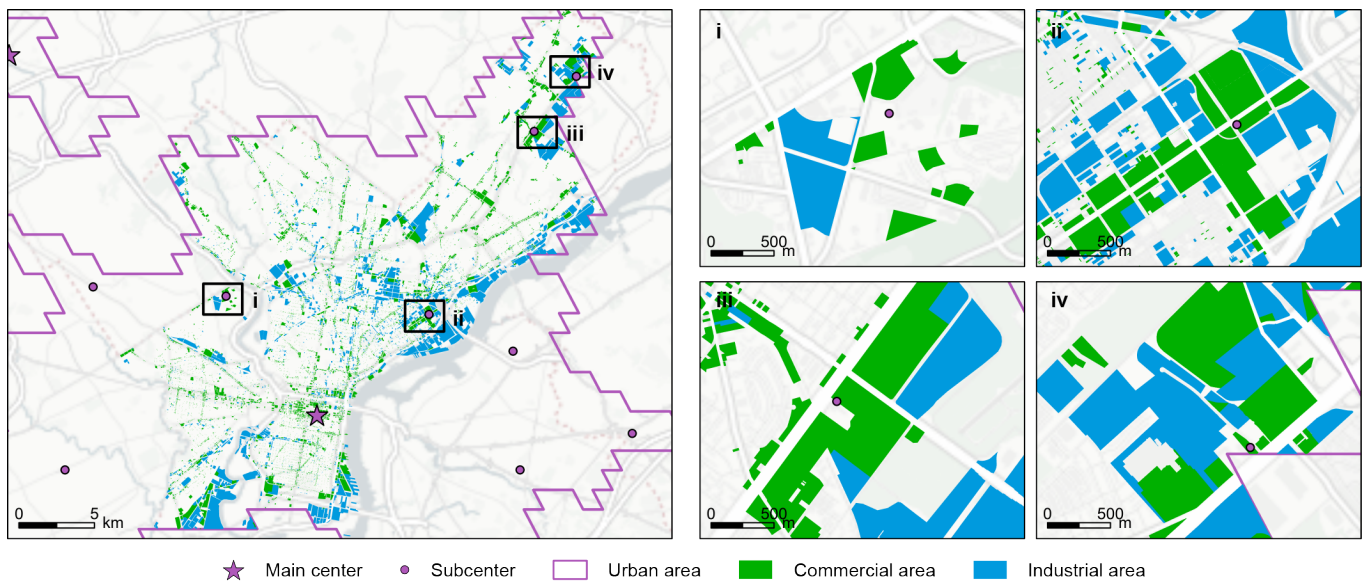
**Extended Data Figure 5.** Comparison between identified urban centers and planned centers in city master plans for Seattle, Portland, Beijing, and London. Three of three disjoint planned centers in Seattle, seven of nine in Portland, 14 of 15 in Beijing, and six of seven in London are matched by identified urban centers (located within or less than 1 km from the planned centers). Data sources: Seattle 2035 Comprehensive Plan (urban centers); Portland 2040 Growth Concept (central and regional centers); Beijing Urban Master Plan 2020 (subcenters and new towns); and London Plan 2021 (international and metropolitan centers, excluding strategic regeneration areas).



**Extended Data Figure 6.** Cities without identified urban centers. **(a)** The spatial distribution of cities lacking nighttime light-based urban centers. **(b)** Regional composition. Most (87%) of the non-centered urban areas are located in Sub-Saharan Africa, East Asia & Pacific and South Asia.



**Extended Data Figure 7.** Population, built-up area, nighttime light and satellite imagery of the non-centered urban areas. Some populated settlements without marked economic agglomeration fail to form urban centers (a, b, c); Cities that have patchy electricity supply may not translate urban vitality into strong light emissions (d). The satellite imagery from Google.



**Extended Data Figure 8.** Identified urban centers and land use in Philadelphia, United States. Areas surrounding the urban centers typically comprise both commercial and industrial land, reflecting mixed-use functional types. Land use data are from OpenDataPhilly (City of Philadelphia).